THE CONTRIBUTION OF SENTINEL-1 DINSAR TO THE DETERMINATION OF VERTICAL DEFORMATION AND HEIGHT SYSTEM MONITORING

A.I. Triantafyllou[1], G.S. Vergos[2], I.N. Tziavos[3]

1Laboratory of Gravity Field Research and Applications – GravLab, Department of Geodesy and Surveying, Aristotle University of Thessaloniki, Thessaloniki, Greece (anastria.thess@gmail.com)

2Laboratory of Gravity Field Research and Applications – GravLab, Department of Geodesy and Surveying, Aristotle University of Thessaloniki, Thessaloniki, Greece (vergos@topo.auth.gr)

3Laboratory of Gravity Field Research and Applications – GravLab, Department of Geodesy and Surveying, Aristotle University of Thessaloniki, Thessaloniki, Greece (tziavos@topo.auth.gr)

Key words: *SAR; Sentinel-1; vertical datum; benchmark potential values; time evolution*

ABSTRACT

The city of Thessaloniki in Northern Greece has become a highly populated and heavily industrialized region. Due to its geographic location and geophysical seating, the city is dominated by almost continuous, but low in magnitude, tectonic activity, suggesting that the area must be subject to small but important displacements. The main objective of this study is to exploit the DInSAR technique for the detection and monitoring of those deformation phenomena, focusing on the vertical component, using data acquired by the Sentinel-1 constellation of satellites. A large set of ascending C-band Sentinel1-SAR images, covering the period between 2016 and 2018, was used for this purpose. To investigate the improvement of the interferometric deformation measurements, the SBAS (Small Baseline Subsets) algorithm was used, employing an advanced multi-pass DInSAR technique that combines unwrapped interferograms with small spatial and temporal baselines to minimize the topographic and atmospheric artifacts. The aim of this work is to use the such-derived vertical deformations as an apriori measure of corresponding potential deformations, the latter being the fundamental quantity needed for the definition and realization of a vertical datum. As a final step, prior measurements acquired by CORS GNSS stations located are compared with the DInSAR estimates to assess a more precise and validated vertical ground deformation model of the area.

I. INTRODUCTION

Differential Synthetic aperture radar interferometry (DInSAR) is a unique technique used to exploit quantitative measurements of the ground deformation phenomena with high spatial resolution and cm accuracy. These estimations are based on representations of phase differences between SAR acquisitions that cover the same area but were acquired at different times, called interferograms. Processing a number of interferograms can lead to the isolation of the signal component emanated from surface movement (Barra et al., 2017).

Until now, this method was lacking temporal resolution due to the limited and irregular time-series that were provided by SAR satellites. Yet, since the launch of the Sentinel-1 satellite mission, there was an important increase in the available SAR images, thus an improvement in their temporal and spatial coverage (Barra et al., 2017).

Despite this, DInSAR has still its own peculiarities, including a few major disadvantages, as a geodetic technique. The derived information is referred to an oblique direction, called Line Of Sight (LOS), and, moreover, is the relative determination between two contextual epochs. Therefore, several reductions, assumptions and a high resolution Digital Elevation Model (DEM) must be combined in order to obtain useful estimations (Duro, Albiol, Mora, & Payàs, 2013).

There are some factors that cause disturbance in interferograms too, such as atmospheric artifacts. Variations of air pressure, temperature and water vapor content are observed between different acquisition dates causing changes along the path of the SAR signal. Such delays have an important impact on the interferogram formations and are considered as the most difficult to reduce (Mouratidis et al., 2010).

The purpose of this study is to implement long time series of Sentinel-1 SAR acquisitions for DInSAR time series analysis in order to monitor ground vertical deformation phenomena that take place in the broader area of Thessaloniki and consequently to estimate their impact in potential and orthometric height variations with time. To accomplish that, we followed a processing chain that provided the reduction of the signal's error and the projection of the LOS displacements to the vertical vector. In order to evaluate the accuracy of the method, the obtained information was compared to continuous GPS measurements provided by Bitharis et al. (2017).

II. STUDY AREA

Thessaloniki is a metropolitan region with over one million inhabitants. The broader area (Figure 1) is located in Northern Greece and lies between the north coast of Thermaikos Gulf and the mountain Vertiskos. A number of studies have revealed that subsidence and uplift phenomena have been observed throughout the years in the area (Mouratidis et al., 2010; Savvaidis, Ifadis, & Doukas, 2006). Most of these studies focus on specific regions where natural or anthropogenic activities and environmental changes have taken place, such as the Mygdonia and Anthemountas basin and the Kalochori district.

Mygdonia basin is located in the northern vicinity of Thessaloniki and is considered as one of the most active seismogenic regions in Greece (Papazachos, Vamvakaris, Vargemezis, & Aidona, 2001). The area is dominated by almost continuous, but low in magnitude, tectonic activity with a NW-SE to E-W trend and was the epicentral of the major earthquake in 1979 (Mw=7.6) (Raucoules et al., 2008).

Kalochori is a small village located in the western outskirts of the city of Thessaloniki next to the large deltaic complex that is formed by the rivers Axios, Aliakmonas, Gallikos and Loudias (Loupasakis & Rozos, 2010). Over the last decades the wider Kalochori region has become a major industrial area leading to excessive exploitation of the natural aquifers. At the same time, the Water Supply and Sewage authority of Thessaloniki performed various drillings there in this region, in order to supply water to the city. Since then, major environmental and morphological changes have been observed in the area including the creation of the Kalochori lagoon, which was the result of land subsidence (Vareltzidou & Strixner, 2009).

Similar land subsidence and uplift phenomena extend over the broader area presenting low deformation rates. Unfortunately, in the majority of the cases, these incidences remain unnoticed by local authorities until intense damages take place. Such was the case of Anathemountas basin where infrastructure and buildings have been damages in 2005 (Bitharis et al., 2017; Raspini, Loupasakis, Rozos, & Moretti, 2013)

According to Bitharis et al. (2017), who processed data from 185 European GNSS stations with a 3 to 7 years' time span, these deformation rates range from -1.5 mm/year to +2 mm/year in Thessaloniki region as shown in Figure 2. The negative values represent subsidence and can be detected in the western, eastern and southern part of the area of interest, whereas positive values, which represent uplift, are found within the city center and in its Northern part. The latter is also supported by Svigkas et al. (2017)who found uplift in the Northern part of the city.

Figure 1. Sentinel-2 satellite image of the broader area of Thessaloniki

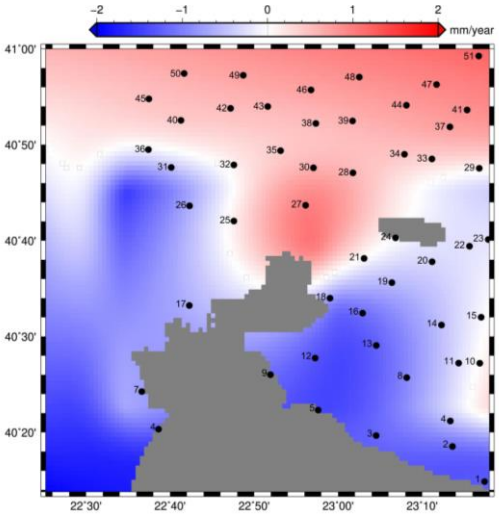

Figure 2. Vertical deformation rates (velocities) derived from GPS data (with adaptations from Bitharis et al. (2017)). Each point represents the places where the permanent GNSS stations, used later as benchmarks, are located.

III. INPUT DATA AND ANALYSIS METHOD

DInSAR time series analysis is considered as a unique tool for the estimation of the deformation rates that occur through time and space as well as their temporal features (Berardino, Fornaro, Lanari, & Sansosti, 2002). There are different methods that are used for this purpose such as the Persistent Scatterer (PS) (Ferretti, Prati, & Rocca, 2000) and the Small Baseline Subset (SBAS) (Berardino et al., 2002) which was employed in this study.

The use of the latter requires a number of SAR-images that are characterized by small spatial and temporal baseline. The algorithm is comprised of several sequential sub-steps that are schematically depicted in Figure 3. SLC (Single Look Complex) SAR images, orbital information and a high resolution DEM are used as the input data of the process. Each image

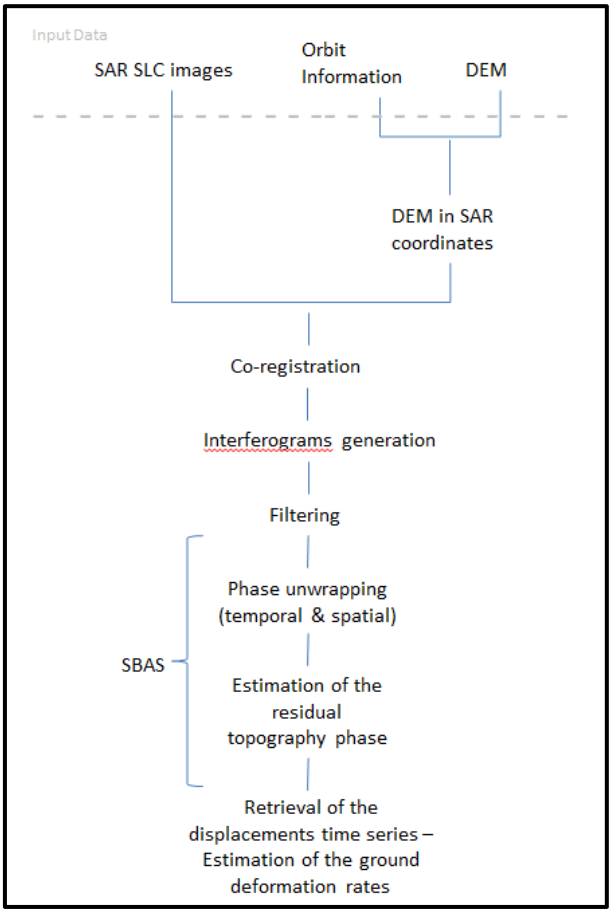

Figure 3.The applied processing chain

must be referred to the same spatial grid in order to ensure that each image pixel corresponds to the right ground targets. This procedure, called co-registration, is carried out using both the orbital and the topography (referred in SAR geometry) information and its success is very important for the process chain (Zinno et al., 2015).

After co-registration, interferometric pairs are selected in proportion to the spatial (orbital) and temporal separation of the SLC images. From each pair an interferogram is formed which demonstrates the estimated phase shift. Once the generation of the interferograms is completed, SBAS algorithm is applied.

SBAS is divided in two stages and it is the algorithm that leads to the displacement time series estimation. First of all, the estimated phase shift is unwrapped through the extended minimum cost flow (EMCF) phase unwrapping (PhU) approach, in order to retrieve its full evolution (Zinno et al., 2015). Then, the unwrapped phase incurred a pixel-based inversion using the Singular Value Decomposition (SVD) leading to the estimation of the deformation time series and the deformation rates (Zinno et al., 2015).

The processing chain, which was described above, was followed throughout the study to derive the ground deformation time series and their rates. A large data set of ascending Sentinel-1A and -1B SLC SAR images, covering a period of time between 2016 and 2018, was used for this purpose (Table 1). The satellite images were paired sequentially generating 82 phase interferograms through the GMT5SAR software (Sandwell et al., 2016). All interferometric pairs were characterized by small temporal and perpendicular baselines (fewer than 15 days and 100 m respectively) and were exempted from the topographic effects using a SRTM1 DEM. Once the SBAS algorithm was carried out, deformation values for every 12 days were derived. These values refer to the LOS of the satellite. Therefore, their transformation to the vertical direction was required.

Table 1.The employed data of the study

Satellite	Acquisition Date	Satellite	Acquisition Date
S-1A	11-Jan-16	S-1A	04-Jul-17
S-1A	23-Jan-16	S-1A	16-Jul-17
S-1A	16-Feb-16	S-1A	28-Jul-17
S-1A	28-Feb-16	S-1A	09-Aug-17
S-1A	11-Mar-16	S-1A	21-Aug-17
S-1A	23-Mar-16	S-1A	02-Sep-17
S-1A	16-Apr-16	S-1A	14-Sep-17
S-1A	28-Apr-16	S-1A	26-Sep-17
S-1A	10-May-16	S-1A	08-Oct-17
S-1A	03-Jun-16	S-1A	20-Oct-17
S-1A	15-Jun-16	S-1A	01-Nov-17
S-1A	09-Jul-16	S-1A	13-Nov-17
S-1A	21-Jul-16	S-1A	25-Nov-17
S-1A	02-Aug-16	S-1A	07-Dec-17
S-1A	14-Aug-16	S-1A	19-Dec-17
S-1A	26-Aug-16	S-1A	31-Dec-17
S-1A	07-Sep-16	S-1B	06-Jan-18
S-1A	19-Sep-16	S-1B	18-Jan-18
S-1A	01-Oct-16	S-1A	30-Jan-18
S-1A	13-Oct-16	S-1A	05-Feb-18
S-1A	25-Oct-16	S-1B	23-Feb-18
S-1A	06-Nov-16	S-1B	07-Mar-18
S-1A	18-Nov-16	S-1B	19-Mar-18
S-1A	30-Nov-16	S-1B	31-Mar-18
S-1B	14-Dec-16	S-1B	12-Apr-18
S-1A	24-Dec-16	S-1B	24-Apr-18
S-1A	05-Jan-17	S-1B	06-May-18
S-1A	17-Jan-17	S-1B	18-May-18
S-1A	29-Jan-17	S-1B	30-May-18
S-1A	10-Feb-17	S-1B	11-Jun-18
S-1A	22-Feb-17	S-1B	23-Jun-18
S-1A	06-Mar-17	S-1B	05-Jul-18
S-1A	18-Mar-17	S-1B	17-Jul-18
S-1A	30-Mar-17	S-1B	29-Jul-18

S-1A	11-Apr-17	S-1B	10-Aug-18
S-1A	23-Apr-17	S-1B	22-Aug-18
S-1A	05-May-17	S-1B	03-Sep-18
S-1A	17-May-17	S-1B	15-Sep-18
S-1A	29-May-17	S-1B	27-Sep-18
S-1A	10-Jun-17	S-1B	09-Oct-18
S-1A	22-Jun-17		

The LOS of the Sentinel-1 satellites is typically varying from 15° to 45° in respect of the vertical direction. According to Hanssen (2001) the LOS measurement (d_{LOS}) is the 3D vector of the components in the North, East and Up direction (dn, de, du):

$$d_{LOS} = d_u \cos\theta_{inc} + d_n \sin a_h + d_e \cos a_h \qquad (1)$$

where θ_{inc} = incidence angle
a_h = the azimuth of the satellite orbit

Due to the fact that the InSAR observations are more sensitive to the vertical component, the value of the horizontal component was not considered in this study. For an average incidence angle ($\theta_{inc} = 27°\sim32°$, depending on the acquisition), the LOS were transformed into vertical estimations, which, as displayed in Figure 4, bear a resemblance with each other with generally differences less than ± 2mm.

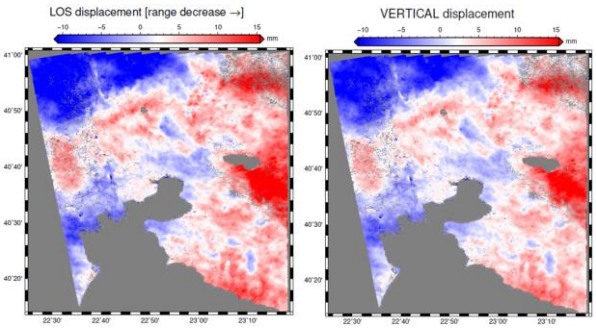

Figure 4.The deformation estimations in the LOS (left) and the vertical direction (right) using SLC two images acquired in the 6th and 18th of January 2018.

Using the vertical displacement values, we formed the corresponding deformation maps, which refer to a 12-day period of time. In Figure 5, four of those maps are presented. These maps display the vertical displacements that were estimated for February and March of 2017.

Within the aforementioned period only subsidence phenomena can be detected, ranging from -20 mm to -5 mm. Between each acquisition date, there is a consistent pattern of small displacement observations in some areas, such as the Anthemountas basin and Kalochori. On the contrary, in rural and urban areas, where the coherence level is quite low (Fanelli, Santoro, Vitale, Murino, & Askne, 2000; Wei & Sandwell, 2010), great fluctuation is observed.

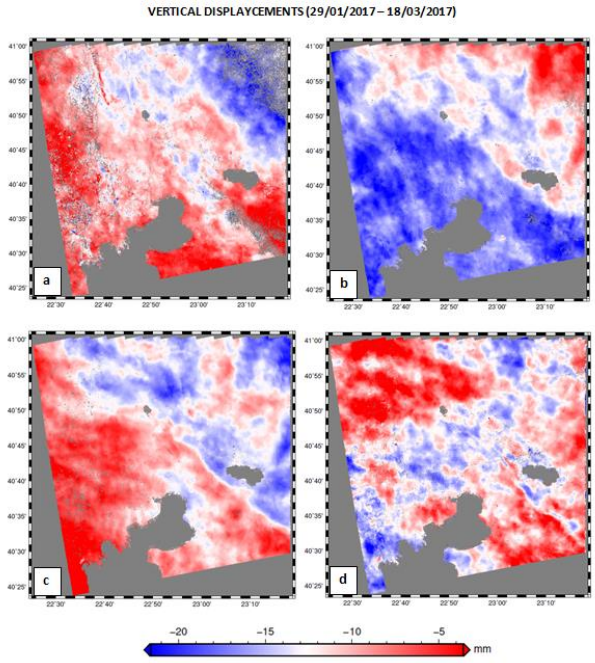

Figure 5.The vertical deformation estimations between the following acquisition dates: 29/01/2017 - 10/02/2017(a), 10/2/2017 - 22/02/2017(b), 22/02/2017 - 06/03/2017(c), 06/03/2017 - 18/03/2017 (d)

Measurements of the ground deformation phenomena based on individual interferograms are also affected by atmospheric artifact. Using the SBAS multi-interferogram technique, we managed to minimize these errors. More specifically, according to Ferretti et al., 2001, the atmospheric component can be computed using space-time filtering steps to the interferometric time-series, due to the fact that atmospheric effects are more related to space than time. The first step includes a low-pass filter in the 2-D spatial domain and it is followed by a high-pass temporal filter. The derived vertical velocities are presented in Figure 6.

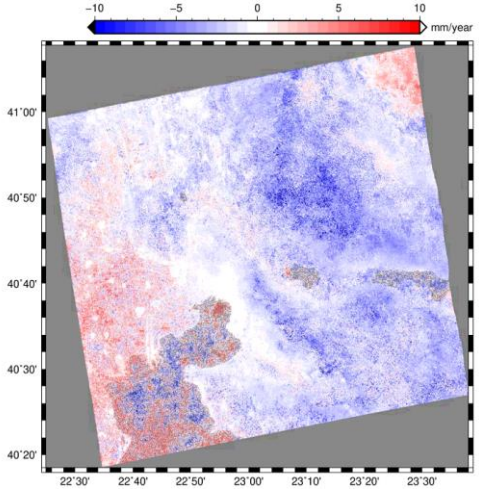

Figure 6.The SBAS-derived vertical velocities

The derived velocities are extremely high, almost ±10mm/year, especially in areas characterized by low coherence. It is clear that those values are affected by vegetation and topographic decorrelation phenomena and they do not describe the real deformation trend of the area. The noisy areas have a coherence threshold lower than 0.8. (Lu, Ni, Chang, Yen, & Chuang, 2018) and therefore they have been excluded. The exclusion of data with low coherence resulted in blank (no data) areas, located mostly at the deltaic complex of Axios and Aliakmonas rivers where the majority of the noisy areas with low accuracy measurements have been spotted (Figure 7a).

IV. RESULTS

In order to estimate the accuracy of the derived values, a comparison with data from GNSS observations was made. For this purpose we used the velocity values that were derived through the execution of the SBAS algorithm and evaluated their agreement with the corresponding data provided by Bitharis et al. (2017). The deformation rates obtained from the SAR and the GNSS data are presented in Figures 7 and 2, respectively.

The derived velocities seem to agree with the provided data. The negative rates (< -2mm/year), that indicate subsidence, are detected at the southern part of the region, while an uplift trend (> 6mm/year) is observed close to the city of Thessaloniki and at the northern part of the broader region.

The black dots on the velocity maps, which we are going to refer to as benchmarks, represent the places of the 51 permanent GNSS stations (see Figure 2). Measurements from these stations were used for the estimation of the GPS-derived ground velocities providing high-accuracy subsidence/uplift point estimations. For a better comparison between the two data sets, the difference between the vertical velocities at these specific benchmarks was carried out. The estimated velocities and their absolute differences are listed in Table 2.

The majority of the SAR-velocities are similar to the GPS-derived ones. Their absolute differences range from 0.02 mm/year to 1.46 mm/year. The largest differences are detected at the north-east part of the area (Mygdonia Basin) where the GNSS data have measured an uplift trend whereas the SAR velocities imply subsidence phenomena.

Close to Anthemountas basin, both datasets have detected a subsidence trend of about -2mm/year. At the Kalochori area, although there was no benchmark, is clear that the derived deformation rates show an uplift trend which contrasts with the subsidence phenomena recorded in the relative literature (Loupasakis & Rozos, 2010; Raucoules et al., 2008). At the delta plain of Axios and Aliakmonas, where Bitharis et al. (2017) have detected subsidence rates, no comparison can be made due to the fact that most of the SAR values were characterized by coherence <0.8 and therefore they were not geocoded.

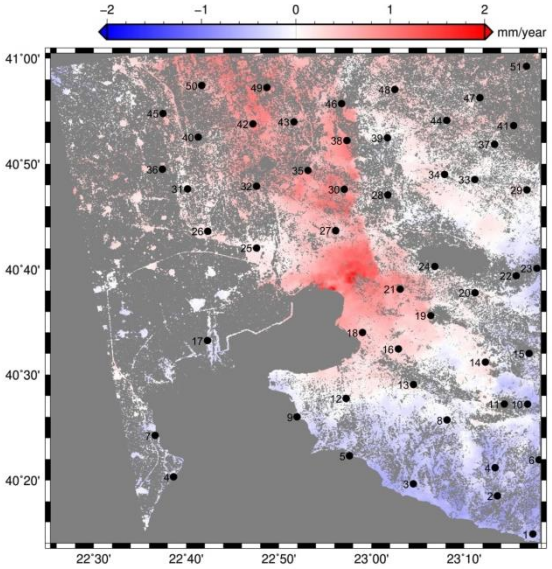

Figure 7.The deformation rates estimations [mm/year] using SAR-SLC images

Table 2. The vertical ground velocities at the benchmarks. Unit: [mm/yr]

Point ID	GNSS	SAR	Absolute Differences
1	-1.288	-0.451	0.836
2	-1.103	-0.472	0.631
3	-1.194	-0.429	0.765
4	-1.133	-	-
5	-0.51	-0.53	0.02
6	-	-0.379	-
7	-1.44	-0.295	1.145
8	-0.924	-0.099	0.825
9	-1.138	-0.105	1.033
10	0.034	-0.442	0.476
11	-0.251	-0.076	0.175
12	-1.321	0.028	1.349
13	-1.235	-0.032	1.203
14	-0.486	0.17	0.656
15	-0.071	-0.14	0.068
16	-1.116	0.342	1.457
17	-0.623	-0.014	0.609
18	-0.743	0.435	1.178
19	-0.542	-	-
20	-0.309	0.118	0.427

21	-0.008	0.721	0.728
22	-0.229	-	-
23	-0.21	-0.356	0.147
24	-0.033	0.18	0.213
25	0.116	0.095	0.021
26	-0.638	-	-
27	0.986	0.526	0.46
28	0.563	-	-
29	0.082	-	-
30	0.614	0.873	0.258
31	-0.464	0.148	0.612
32	0.116	0.553	0.437
33	0.349	0.002	0.347
34	0.443	0.067	0.376
35	0.407	0.729	0.322
36	-0.097	-	-
37	0.728	0.149	0.579
38	0.526	0.876	0.35
39	0.598	-	-
40	0.401	0.503	0.103
41	0.862	0.245	0.616
42	0.518	0.872	0.354
43	0.565	0.426	0.138
44	0.784	0.237	0.547
45	0.478	0.449	0.029
46	0.724	-	-
47	0.944	-	-
48	0.873	0.279	0.593
49	0.721	0.809	0.088
50	0.65	0.57	0.08
51	1.162	0.44	0.722

V. CONCLUTIONS

Overall, the GNSS and DInSAR derived velocities seem to be in close agreement considering the fact that they refer to different time periods. The mean absolute difference between the two data sets is 0.5 mm/year, whereas in areas characterized by low coherence the differences soar up to 1.5 mm/year. This is a positive fact, since deformation velocities are considered as a very useful tool for the adjustment of the multivariate height systems such the one that is established in Greece. Our results imply that using long SAR time series it is possible to derive accurate geometrical deformation rates in large areas with high spatial resolution, even though they lack the temporal resolution provided by permanent GNSS stations. Moreover, due to the fact that several assumptions were made in this study in order to simplify the process chain, we believe that more accurate results can be achieved following advanced methodologies thus enhancing the monitoring of the potential and orthometric height variations with time.

References

Barra, A., Solari, L., Béjar-Pizarro, M., Monserrat, O., Bianchini, S., Herrera, G., … Moretti, S. (2017). A methodology to detect and update active deformation areas based on Sentinel-1 SAR images. *Remote Sensing*, *9*(10). https://doi.org/10.3390/rs9101002

Berardino, P., Fornaro, G., Lanari, R., & Sansosti, E. (2002). A New Algorithm for Surface Deformation Monitoring Based on Small Baseline Differential SAR Interferograms. *IEEE Transactions on Geoscience and Remote Sensing*, *40*(11), 2375–2383. https://doi.org/10.4088/JCP.12m08269

Bitharis, S., Ampatzidis, D., Pikridas, C., Fotiou, A., Rossikopoulos, D., & Schuh, H. (2017). The Role of GNSS Vertical Velocities to Correct Estimates of Sea Level Rise from Tide Gauge Measurements in Greece. *Marine Geodesy*, *40*(5), 297–314. https://doi.org/10.1080/01490419.2017.1322646

Duro, J., Albiol, D., Mora, O., & Payàs, B. (2013). Application of advanced InSAR techniques for the measurement of vertical and horizontal ground motion in longwall minings. In *13th Coal Operators' Conference, University of Wollongong, The Australasian Institute of Mining and Metallurgy & Mine Managers Association of Australia* (pp. 99–106). Retrieved from http://ro.uow.edu.au/coal/442/

Fanelli, A., Santoro, M., Vitale, A., Murino, P., & Askne, J. (2000). Understanding ERS Coherence over Urban Areas. In *ESA ERS - Envisat Symposium Looking down to Earth in the NEW Millennium* (pp. 2268–2275).

Ferretti, A., Prati, C., & Rocca, F. (2000). Nonlinear subsidence rate estimation using permanent scatterers in differential SAR interferometry. *IEEE Transactions on Geoscience and Remote Sensing*, *38*(5 I), 2202–2212. https://doi.org/10.1109/36.868878

Ferretti, A., Prati, C., & Rocca, F. (2001). Permanent scatterers in SAR interferometry. *IEEE Transactions on Geoscience and Remote Sensing*, *39*(1), 8–20. https://doi.org/10.1109/36.898661

Hanssen, R. F. (2001). *Radar Interferometry: Data Interpretation and Error Analysis*. *Scientific American* (Vol. 276). https://doi.org/10.1007/0-306-47633-9

Loupasakis, C., & Rozos, D. (2010). Land subsidence induced by the overexploitation of the aquifers in Kalochori village – new approach by means of the computational geotechnical engineering. *Bulletin of the Geological Society of Greece*, *43*((3)), 1219–1229. https://doi.org/10.12681/bgsg.11298

Lu, C.-H., Ni, C.-F., Chang, C.-P., Yen, J.-Y., & Chuang, R. (2018). Coherence Difference Analysis of Sentinel-1 SAR Interferogram to Identify Earthquake-Induced Disasters in Urban Areas. *Remote Sensing*, *10*(8), 1318. https://doi.org/10.3390/rs10081318

Mouratidis, A., Briole, P., Astaras, A., Pavlidis, S., Tsakiri, M., Ilieva, M., & Rolandone, F. (2010). Contribution of Insar and Kinematic Gps Data To Subsidence and Geohazard

Monitoring in Central Macedonia (N . Greece). In *Scientific Annals, School of Geology, Aristotle University of Thessaloniki Proceedings of the XIX CBGA Congress, Thessaloniki, Greece* (Vol. 100, pp. 535–545).

Papazachos, C. B., Vamvakaris, D. A., Vargemezis, G. N., & Aidona, E. V. (2001). A study of the active tectonics and deformation in the Mygdonia basin (N. Greece) using seismological and neotectonic data. *Bulletin of the Geological Society of Greece*, *34*(1), 303. https://doi.org/10.12681/bgsg.17027

Raspini, F., Loupasakis, C., Rozos, D., & Moretti, S. (2013). Basin and local scale detection of ground subsidence through persistent scatterer interferometry: the Anthemountas basin (northern Greece) case study. In *Bulletin of the Geological Society of Greece, Proceedings of the 13th International Congress, Chania* (Vol. XLVII, pp. 1510–1518).

Raucoules, D., Parcharidis, I., Feurer, D., Novalli, F., Ferretti, A., Carnec, C., … Hosford, S. (2008). Ground deformation detection of the greater area of Thessaloniki (Northern Greece) using radar interferometry techniques. *Natural Hazards and Earth System Science*, *8*(4), 779–788. https://doi.org/10.5194/nhess-8-779-2008

Sandwell, D., Mellors, R., Tong, X., Xu, X., Wei, M., & Wessel, P. (2016). *GMTSAR: An InSAR Processing System Based on Generic Mapping Tools (Second Edition)*.

Savvaidis, P., Ifadis, I., & Doukas, I. (2006). Ground subsidence due to water pumping in the area of Thessaloniki, Hellas. In *Modern technologies, education and professional practice in geodesy and related fields*.

Svigkas, N., Papoutsis, I., Loupasakis, C., Tsangaratos, P., Kiratzi, A., & Kontoes, C. H. (2017). InSAR time-series monitoring of ground displacement trends in an industrial area (Oreokastro—Thessaloniki, Greece): detection of natural surface rebound and new tectonic insights. *Environmental Earth Sciences*, *76*(5), 1–18. https://doi.org/10.1007/s12665-017-6517-9

Vareltzidou, S., & Strixner, L. (2009). Recommended Strategic Plan For maintaining favourable conservation status of Natura 2000 areas in the Axios Delta(2009-2013). Retrieved from http://www.fosonline.org/wordpress/wp-content/uploads/2012/09/Strategic_Plan_for_Axios_Delta_Greece.pdf

Wei, M., & Sandwell, D. T. (2010). Decorrelation of L-band and C-band interferometry over vegetated areas in California. *IEEE Transactions on Geoscience and Remote Sensing*, *48*(7), 2942–2952. https://doi.org/10.1109/TGRS.2010.2043442

Zinno, I., Elefante, S., Mossucca, L., De Luca, C., Manunta, M., Terzo, O., … Casu, F. (2015). A First Assessment of the P-SBAS DInSAR Algorithm Performances Within a Cloud Computing Environment. *IEEE Journal of Selected Topics in Applied Earth Observations and Remote Sensing*, *8*(10), 4675–4686. https://doi.org/10.1109/JSTARS.2015.2426054